

Superfluid Phase Transitions and Effects of Thermal Pairing Fluctuations in Asymmetric Nuclear Matter

Hiroyuki Tajima¹, Tetsuo Hatsuda^{2,1}, Pieter van Wyk,³ and Yoji Ohashi³

¹*Quantum Hadron Physics Laboratory,*

RIKEN Nishina Center, Wako, Saitama 351-0198, Japan

²*Interdisciplinary Theoretical and Mathematical Sciences Program (iTHEMS),*

RIKEN, Wako, Saitama 351-0198, Japan and

³*Department of Physics, Keio University,*

Hiyoshi, Kohoku-ku, Yokohama, 223-8522, Japan

Abstract

We investigate superfluid phase transitions of asymmetric nuclear matter at finite temperature (T) and density (ρ) with a low proton fraction ($Y_p \leq 0.2$) which is relevant to the inner crust and outer core of neutron stars. A strong-coupling theory developed for two-component atomic Fermi gases is generalized to the four-component case and is applied to the system of spin-1/2 neutrons and protons. The empirical phase shifts of neutron-neutron (nn), proton-proton (pp) and neutron-proton (np) interactions up to $k = 2 \text{ fm}^{-1}$ are described by multi-rank separable potentials. We show that (i) the critical temperature of the neutron superfluidity T_c^{nn} at $Y_p = 0$ agrees well with Monte Carlo data at low densities and takes a maximum value $T_c^{\text{nn}} = 1.68 \text{ MeV}$ at $\rho/\rho_0 = 0.14$ with $\rho_0 = 0.17 \text{ fm}^{-3}$, (ii) the critical temperature of the proton superconductivity T_c^{pp} for $Y_p \leq 0.2$ is substantially suppressed at low densities due to np-pairing fluctuations and starts to dominate over T_c^{nn} only above $\rho/\rho_0 = 0.70$ (0.77) for $Y_p = 0.1$ (0.2), and (iii) the deuteron condensation temperature T_c^{d} is suppressed at $Y_p \leq 0.2$ due to the large mismatch of the two Fermi surfaces.

PACS numbers: 03.75.Ss, 26.60.Gj, 24.10.Cn

I. INTRODUCTION

The superfluidity in strongly interacting Fermi systems has attracted much attention both theoretically and experimentally. For reviews, we refer to Refs. [1, 2] in nuclear physics, Refs. [3–5] in astrophysics, as well as Refs. [6–10] in condensed matter physics. It has been also recognized that the dilute neutron matter and two-component ultracold atomic fermions near the unitarity have close similarity to each other, due to the strong pairing interactions associated with the large negative neutron-neutron scattering length $a_s = -18.5$ fm and relatively small effective range $r_{\text{eff}} = 2.7$ fm (see Refs. [6–10] and references therein). In the latter atomic system, the pairing interaction can be described by a zero-range potential with a large scattering length [11]. In strongly interacting systems, such as neutron matter and unitary Fermi gases, effects of pairing fluctuations near the superfluid phase transition are particularly important. Such effects have extensively been studied in cold Fermi gas physics through the observations of various quantities, such as single-particle excitation spectrum, specific heat, superfluid phase transition temperature (T_c), shear viscosity, and spin susceptibility [10, 12, 13]. Three of the present authors have recently shown [14] that a strong coupling theory, being based on the one developed by Nozières and Schmitt-Rink (NSR) [15] can provide a unified description of neutron matter and an ultracold Fermi gas in the unitary regime. This indicates that the latter atomic gas system can be used as a quantum simulator for neutron star interiors at subnuclear densities.

There are, however, some issues to be overcome for better understanding of the physics of neutron star interiors: Besides neutrons, one should also include a non-zero fraction Y_p of protons. To deal with this, one needs to extend strong-coupling theories developed for two-component atomic Fermi gases to the four-component case involving spin and isospin degrees of freedom. In such a system, not only a neutron-neutron (nn) interaction but also a proton-proton (pp) interaction, as well as a neutron-proton (np) interaction, work. In particular, the np interaction in the deuteron channel is stronger than the other interactions, so that it may affect the onset of proton superconductivity. Furthermore, the short-range repulsion of the nuclear force is important to describe the pairing phenomena around the nuclear matter density. In this paper, we will consider all these points and study the critical temperature of the superfluid phase transitions in asymmetric nuclear matter around the nuclear saturation density $\rho_0 = 0.17 \text{ fm}^{-3}$, by including the nn, pp and np pairing fluctuations.

This paper is organized as follows. In Sec. II, we present our model for asymmetric nuclear matter, as well as details of our strong coupling scheme. In Sec. III, we show our numerical results for the critical temperatures associated with the nn, pp and np pairings as functions of nucleon density and proton fraction. In this paper, we set $\hbar = k_B = 1$, and the system volume is taken to be unity, for simplicity.

II. FORMALISM

A. Effective Hamiltonian

We introduce the pair operator S_m (T_ℓ) in the spin-singlet–isospin-triplet (spin-triplet–isospin-singlet) channel with the relative momentum \mathbf{k} and the center of mass momentum \mathbf{q} :

$$S_m(\mathbf{k}, \mathbf{q}) = \sum_{\lambda, \rho} \sum_{i, j} \left\langle \frac{1}{2} \frac{1}{2} \lambda \rho \middle| 00 \right\rangle \left\langle \frac{1}{2} \frac{1}{2} i j \middle| 1m \right\rangle c_{-\mathbf{k}+\mathbf{q}/2, \lambda, i} c_{\mathbf{k}+\mathbf{q}/2, \rho, j} \quad (1)$$

$$T_\ell(\mathbf{k}, \mathbf{q}) = \sum_{\lambda, \rho} \sum_{i, j} \left\langle \frac{1}{2} \frac{1}{2} \lambda \rho \middle| 1\ell \right\rangle \left\langle \frac{1}{2} \frac{1}{2} i j \middle| 00 \right\rangle c_{-\mathbf{k}+\mathbf{q}/2, \lambda, i} c_{\mathbf{k}+\mathbf{q}/2, \rho, j} \quad (2)$$

Here $c_{\mathbf{k}, \lambda, i}$ is the fermion annihilation operator with momentum \mathbf{k} , spin index $\lambda = \uparrow, \downarrow$ and isospin index $i = p, n$. The Clebsch-Gordan coefficients in the spin and isospin spaces lead to the projection of the pair operator to appropriate channels.

The effective Hamiltonian in these pairing channels can be written as

$$H = \sum_{\mathbf{p}} \sum_{\lambda=\uparrow, \downarrow} \sum_{i=p, n} \xi_{\mathbf{p}, i} c_{\mathbf{p}, \lambda, i}^\dagger c_{\mathbf{p}, \lambda, i} + \frac{1}{2} \sum_{\mathbf{k}, \mathbf{k}', \mathbf{q}} \left[\sum_{m=-1}^{+1} S_m^\dagger(\mathbf{k}, \mathbf{q}) V_s(\mathbf{k}, \mathbf{k}') S_m(\mathbf{k}', \mathbf{q}) + \sum_{\ell=-1}^{+1} T_\ell^\dagger(\mathbf{k}, \mathbf{q}) V_t(\mathbf{k}, \mathbf{k}') T_\ell(\mathbf{k}', \mathbf{q}) \right], \quad (3)$$

where $V_{s(t)}$ is a spin-singlet (triplet) interaction as functions of the momenta, \mathbf{k} and \mathbf{k}' . $\xi_{\mathbf{p}, i} = \frac{\mathbf{p}^2}{2M_i} - \mu_i$ is the kinetic energy, measured from the nucleon chemical potentials μ_i . M_i is the nucleon mass. The explicit form of Eq.(3) is given by

$$H = \sum_{\mathbf{p}} \sum_{\sigma=\uparrow, \downarrow} \sum_{i=n, p} \xi_{\mathbf{p}, i} c_{\mathbf{p}, \sigma, i}^\dagger c_{\mathbf{p}, \sigma, i} + \sum_{\mathbf{k}, \mathbf{k}', \mathbf{q}} \sum_{i=n, p} V_s(\mathbf{k}, \mathbf{k}') c_{\mathbf{k}+\mathbf{q}/2, \uparrow, i}^\dagger c_{-\mathbf{k}+\mathbf{q}/2, \downarrow, i}^\dagger c_{-\mathbf{k}'+\mathbf{q}/2, \downarrow, i} c_{\mathbf{k}'+\mathbf{q}/2, \uparrow, i} + \sum_{\mathbf{k}, \mathbf{k}', \mathbf{q}} \sum_{\sigma=\uparrow, \downarrow} V_t(\mathbf{k}, \mathbf{k}') c_{\mathbf{k}+\mathbf{q}/2, \sigma, n}^\dagger c_{-\mathbf{k}+\mathbf{q}/2, \sigma, p}^\dagger c_{-\mathbf{k}'+\mathbf{q}/2, \sigma, p} c_{\mathbf{k}'+\mathbf{q}/2, \sigma, n}$$

$$\begin{aligned}
& + \frac{1}{2} \sum_{\mathbf{k}, \mathbf{k}', \mathbf{q}} V_s(\mathbf{k}, \mathbf{k}') \left[c_{\mathbf{k}+\mathbf{q}/2, \uparrow, n}^\dagger c_{-\mathbf{k}+\mathbf{q}/2, \downarrow, p}^\dagger + c_{\mathbf{k}+\mathbf{q}/2, \uparrow, p}^\dagger c_{-\mathbf{k}+\mathbf{q}/2, \downarrow, n}^\dagger \right] \\
& \quad \times \left[c_{\mathbf{k}'+\mathbf{q}/2, \uparrow, n} c_{-\mathbf{k}'+\mathbf{q}/2, \downarrow, p} + c_{\mathbf{k}'+\mathbf{q}/2, \uparrow, p} c_{-\mathbf{k}'+\mathbf{q}/2, \downarrow, n} \right] \\
& + \frac{1}{2} \sum_{\mathbf{k}, \mathbf{k}', \mathbf{q}} V_t(\mathbf{k}, \mathbf{k}') \left[c_{\mathbf{k}+\mathbf{q}/2, \uparrow, n}^\dagger c_{-\mathbf{k}+\mathbf{q}/2, \downarrow, p}^\dagger - c_{\mathbf{k}+\mathbf{q}/2, \uparrow, p}^\dagger c_{-\mathbf{k}+\mathbf{q}/2, \downarrow, n}^\dagger \right] \\
& \quad \times \left[c_{\mathbf{k}'+\mathbf{q}/2, \uparrow, n} c_{-\mathbf{k}'+\mathbf{q}/2, \downarrow, p} - c_{\mathbf{k}'+\mathbf{q}/2, \uparrow, p} c_{-\mathbf{k}'+\mathbf{q}/2, \downarrow, n} \right]. \tag{4}
\end{aligned}$$

B. Effective S -wave Interaction

Throughout this paper, we neglect the isospin symmetry breaking in the interaction $V_{s(t)}$ and use the averaged nucleon mass, $M_p = M_n = M = 939$ MeV. Furthermore, we only retain the S -wave part of $V_{s(t)}$ at low energies and introduce a multi-rank separable potential [16–22]

$$V_\alpha^{\text{SEP}}(k, k') = \sum_{N=1}^{N_{\text{max}}} \eta_{\alpha, N} \gamma_{\alpha, N}(k) \gamma_{\alpha, N}(k'), \tag{5}$$

where $\gamma_{\alpha, N}(k) > 0$ is a form factor with the suffix $\alpha = s, t$ representing the spin-singlet ($\alpha = s$) and spin-triplet ($\alpha = t$) channels, respectively. $\eta_{\alpha, N} = \pm 1$ determines the sign of the interaction (e.g., $\eta_{\alpha, N} = -1$ is attractive). We note that the partial wave expansion of the potential reads $V_\alpha(\mathbf{k}, \mathbf{k}') = 4\pi \sum_{L, M} V_\alpha^{(L, M)}(k, k') Y_{LM}(\hat{\mathbf{k}}) Y_{LM}(\hat{\mathbf{k}}')$ with $\alpha = s(t)$. Eq.(5) is a separable approximation of the S -wave contribution, $V_\alpha^{(0,0)}(k, k')$. Such a separable potential has been successfully applied to various nuclear systems [14, 23–33].

The simplest case is the rank-one separable potential (SEP1), which is given by setting $j_{\text{max}} = 1$ and $\eta_{\alpha, 1} = -1$ in Eq. (5). A typical example of SEP1 is the Yamaguchi potential [16],

$$V_\alpha^{\text{SEP1}}(k, k') = \eta_{\alpha, 1} \gamma_{\alpha, 1}(k) \gamma_{\alpha, 1}(k') = -\frac{u_{\alpha, 1}}{k^2 + \Lambda_{\alpha, 1}^2} \frac{u_{\alpha, 1}}{k'^2 + \Lambda_{\alpha, 1}^2}. \tag{6}$$

The parameters $u_{\alpha, 1}$ and $\Lambda_{\alpha, 1}$ are determined such that the observed values of the scattering length and the effective range in the 1S_0 channel (a_s, r_s) = (-18.5 fm, 2.80 fm), and those in the 3S_1 channel (a_t, r_t) = (5.42 fm, 1.76 fm) can be reproduced:

$$u_{\alpha, 1} = \Lambda_{\alpha, 1}^2 \sqrt{\frac{8\pi}{M} \frac{1}{\Lambda_{\alpha, 1} - 2/a_\alpha}}, \quad \Lambda_{\alpha, 1} = \frac{3 + \sqrt{9 - 16r_\alpha/a_\alpha}}{2r_\alpha}. \tag{7}$$

We summarize the evaluated values of $u_{\alpha, 1}$ and $\Lambda_{\alpha, 1}$ in Table I, as well as the resulting phase shifts denoted by the dashed lines in Fig. 1(a,b). The filled black circles in the

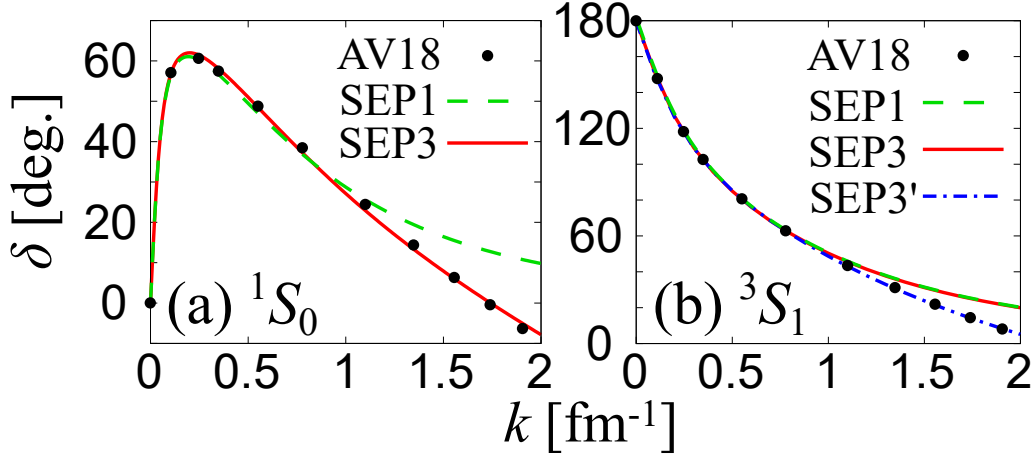


FIG. 1: Phase shifts of (a) 1S_0 neutron-neutron and (b) 3S_1 neutron-proton interaction. In each figure, black dots show the AV18 phase shift in Ref. [34]. SEP1 and SEP3 represent results of the rank-one and rank-three separable potentials, respectively.

figure represent the empirical phase shifts obtained from the high-precision phenomenological potential, AV18 [34]. In the low-momentum region ($k \lesssim 1 \text{ fm}^{-1}$), a reasonable agreement between SEP1 and AV18 is obtained in both 1S_0 and 3S_1 channels, while substantial deficit of the repulsion is seen in the high-momentum region, $k \gtrsim 1 \text{ fm}^{-1}$ in both channels.

A better agreement with AV18 in the high momentum region is obtained in the rank-three separable potential (SEP3), which is given by setting $j_{\text{max}} = 3$, $(\eta_{\alpha,1}, \eta_{\alpha,2}, \eta_{\alpha,3}) = (-1, 1, 1)$ and the form factors as,

$$\gamma_{\alpha,1} = \frac{u_{\alpha,1}}{k^2 + \Lambda_{\alpha,1}^2}, \quad \gamma_{\alpha,2} = \frac{u_{\alpha,2}}{k^2 + \Lambda_{\alpha,2}^2}, \quad \gamma_{\alpha,3} = \frac{u_{\alpha,3}k^2}{(k^2 + \Lambda_{\alpha,3}^2)^2}. \quad (8)$$

In Table I, we summarize the SEP3 parameters determined so as to reproduce the AV18 phase shifts in the range $0 \text{ fm}^{-1} \leq k \leq 2 \text{ fm}^{-1}$, as well as the empirical scattering lengths and effective ranges. As shown in Fig. 1(a), the SEP3 potential (the red line) well reproduces the 1S_0 phase shift δ , even beyond $k \simeq 1.75 \text{ fm}^{-1}$, where δ turns into negative. On the other hand, the SEP3 potential overestimates the phase shift δ in the 3S_1 channel (the red line) in Fig. 1(b) when $k \gtrsim 1 \text{ fm}^{-1}$.

To further improve the agreement, we introduce a SEP3' potential for the 3S_1 channel with the parameters in TABLE I. Here, the AV18 phase shift is fitted in the range $0 \text{ fm}^{-1} \leq k \leq 2 \text{ fm}^{-1}$, without stringent constraint on the empirical value of r_t . Although the effective range and the deuteron binding energy, in SEP3' differ from the empirical values by about

TABLE I: Parameters of rank-one (SEP1) and rank-three (SEP3) separable potentials in 1S_0 ($\alpha = s$) and 3S_1 ($\alpha = t$) channels.

	$u_{\alpha,1}$ [fm $^{-1}$]	$u_{\alpha,2}$ [fm $^{-1}$]	$u_{\alpha,3}$ [fm $^{-1}$]	$\Lambda_{\alpha,1}$ [fm $^{-1}$]	$\Lambda_{\alpha,2}$ [fm $^{-1}$]	$\Lambda_{\alpha,3}$ [fm $^{-1}$]
1S_0 ($\alpha = s$, SEP1)	2.6683	0	0	1.1392	–	–
1S_0 ($\alpha = s$, SEP3)	4.3097	4.5185	104.82	1.3952	2.3202	3.2578
3S_1 ($\alpha = t$, SEP1)	4.4592	0	0	1.4064	–	–
3S_1 ($\alpha = t$, SEP3)	4.4619	0.1631	2.2085	1.4064	2.3455	3.0332
3S_1 ($\alpha = t$, SEP3')	6.3578	1.0956	26.814	1.7071	2.9448	2.7045

TABLE II: Scattering lengths a_α , effective ranges r_α , as well as the binding energy E_d of deuteron for 3S_1 channel with the parametrization shown in TABLE I.

	a_α [fm]	r_α [fm]	E_d [MeV]
1S_0 ($\alpha = s$, SEP1)	-18.50	2.80	–
1S_0 ($\alpha = s$, SEP3)	-18.50	2.80	–
3S_1 ($\alpha = t$, SEP1)	5.42	1.76	-2.22
3S_1 ($\alpha = t$, SEP3)	5.42	1.76	-2.22
3S_1 ($\alpha = t$, SEP3')	5.42	1.91	-2.15

9% and 4%, respectively, (see TABLE II), one sees in Fig. 1(b) that SEP3' (blue dash-dotted line) gives good agreement with AV18 to $k \simeq 2$ fm $^{-1}$. In the following, we employ SEP1, SEP3 and SEP3', to study the superfluid instabilities of asymmetric nuclear matter.

C. Thermodynamic Potential with Pairing Fluctuations

We include strong pairing fluctuations originating from $V_{\alpha=s,t}$ at finite temperatures within the framework of NSR. In this scheme, the so-called strong-coupling corrections $\delta\Omega_{\text{NSR}}$ to the thermodynamic potential Ω are diagrammatically given in Fig. 2. We note that effects of pairing fluctuations for pure neutron matter at zero temperature was previously discussed in [14] by using a rank-one separable interaction. Considering the spin-unpolarized nuclear matter, we introduce the one-particle thermal Green's function in the

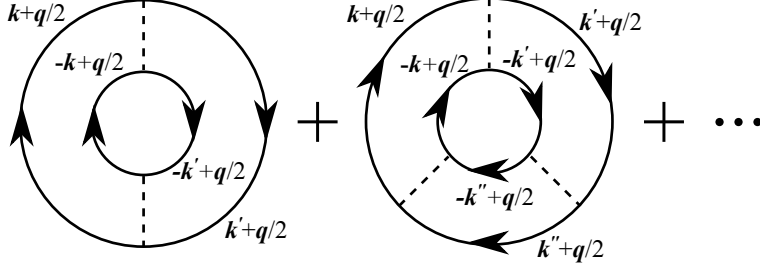


FIG. 2: NSR strong-coupling corrections $\delta\Omega_{\text{NSR}}$ to the thermodynamic potential Ω in asymmetric nuclear matter at nonzero temperatures. The solid and dashed lines denote the nucleon Green's function G_i and the bare nucleon-nucleon interaction $V_\alpha(\mathbf{k}, \mathbf{k}')$, respectively. \mathbf{k} , \mathbf{k}' , and \mathbf{k}'' are relative momenta of nucleons and \mathbf{q} is the center-of-mass momentum of each pair.

Hartree approximation, given by

$$G_{\mathbf{p},i}(i\omega_l) = \frac{1}{i\omega_l - \xi_{\mathbf{p},i} - \Sigma_i^{\text{H}}(\mathbf{p})}. \quad (9)$$

Here, the Hartree self-energy $\Sigma_i^{\text{H}}(\mathbf{p})$ involves the contribution from the diagonal force $V_{\text{D}}^{\text{SEP}}(k, k)$ in the isospin space originating from the nn and pp interactions, as well as that from the off-diagonal force $V_{\text{OD}}^{\text{SEP}}(k, k)$ originating from the np interactions:

$$\Sigma_i^{\text{H}}(\mathbf{p}) = T \sum_{\mathbf{p}', \omega_l} [V_{\text{D}}^{\text{SEP}}(k, k) G_{\mathbf{p}',i}(i\omega_l) + V_{\text{OD}}^{\text{SEP}}(k, k) G_{\mathbf{p}',\bar{i}}(i\omega_l)], \quad (10)$$

$$V_{\text{D}}^{\text{SEP}}(k, k) = V_{\text{s}}^{\text{SEP}}(k, k), \quad (11)$$

$$V_{\text{OD}}^{\text{SEP}}(k, k) = V_{\text{t}}^{\text{SEP}}(k, k) + \frac{1}{2} [V_{\text{s}}^{\text{SEP}}(k, k) + V_{\text{t}}^{\text{SEP}}(k, k)], \quad (12)$$

where $\bar{i}=\text{p(n)}$ for $i=\text{n(p)}$, $k = |\mathbf{p} - \mathbf{p}'|/2$, and $\omega_l = (2l + 1)\pi T$ is the fermion Matsubara frequency.

Introducing the Fermi momentum distribution for given momentum \mathbf{p} in the Hartree approximation,

$$\rho_{\mathbf{p},i}^{\text{H}} = T \sum_{\omega_l} G_{\mathbf{p},i}(i\omega_l), \quad (13)$$

one can write the thermodynamic potential Ω in the NSR theory as,

$$\begin{aligned} \Omega &= \Omega_{\text{H}} + \delta\Omega_{\text{NSR}}, \\ \Omega_{\text{H}} &= 2T \sum_{\mathbf{p},i} \ln [1 + e^{-\xi_{\mathbf{p},i}^{\text{H}}/T}] - \sum_{\mathbf{p},\mathbf{p}',i} [V_{\text{D}}^{\text{SEP}}(k, k) \rho_{\mathbf{p},i}^{\text{H}} \rho_{\mathbf{p}',i}^{\text{H}} + V_{\text{OD}}^{\text{SEP}}(k, k) \rho_{\mathbf{p},i}^{\text{H}} \rho_{\mathbf{p}',\bar{i}}^{\text{H}}], \end{aligned}$$

$$\delta\Omega_{\text{NSR}} = T \sum_{\mathbf{q}, \nu_l} \sum_{\alpha} \sum_{m=0, \pm 1} \text{Tr} \left[\ln \left[1 + \hat{\eta}_{\alpha} \hat{\Pi}_{\alpha}^{(m)}(\mathbf{q}, i\nu_l) \right] - \hat{\eta}_{\alpha} \hat{\Pi}_{\alpha}^{(m)}(\mathbf{q}, i\nu_l) \right]. \quad (14)$$

Here, $\xi_{\mathbf{p}, i}^{\text{H}} = \frac{\mathbf{p}^2}{2M} - \mu_i + \Sigma_i^{\text{H}}(\mathbf{p})$ is the kinetic energy involving the Hartree self-energy $\Sigma_i^{\text{H}}(\mathbf{p})$, measured from the chemical potential μ_i , and $\nu_l = 2\pi l/T$ is the boson Matsubara frequency. $\delta\Omega_{\text{NSR}}$ in Eq. (14) is the strong-coupling correction to Ω associated with pairing fluctuations in the 1S_0 and 3S_1 channels, and $\hat{\eta}_{\alpha} = \text{diag}(\eta_{\alpha,1}, \eta_{\alpha,2}, \dots, \eta_{\alpha, N_{\text{max}}})$. Note that Tr is to take over the rank indices, N . The $N_{\text{max}} \times N_{\text{max}}$ matrix pair-correlation function $\hat{\Pi}_{\alpha}^{(m)}(\mathbf{q}, i\nu_l) = \{[\Pi_{\alpha}^{(m)}(\mathbf{q}, i\nu_l)]_{N, N'}\}$ consists of

$$\left[\hat{\Pi}_{\text{s}}^{(+1)}(\mathbf{q}, i\nu_l) \right]_{N, N'} = T \sum_{\mathbf{k}, \omega_{l'}} \gamma_{\text{s}, N}(\mathbf{k}) \gamma_{\text{s}, N'}(\mathbf{k}) G_{\mathbf{k}+\mathbf{q}/2, \text{p}}(i\omega_{l'} + i\nu_l) G_{-\mathbf{k}+\mathbf{q}/2, \text{p}}(-i\omega_{l'}), \quad (15)$$

$$\left[\hat{\Pi}_{\text{s}}^{(0)}(\mathbf{q}, i\nu_l) \right]_{N, N'} = T \sum_{\mathbf{k}, \omega_{l'}} \gamma_{\text{s}, N}(\mathbf{k}) \gamma_{\text{s}, N'}(\mathbf{k}) G_{\mathbf{k}+\mathbf{q}/2, \text{n}}(i\omega_{l'} + i\nu_l) G_{-\mathbf{k}+\mathbf{q}/2, \text{p}}(-i\omega_{l'}), \quad (16)$$

$$\left[\hat{\Pi}_{\text{s}}^{(-1)}(\mathbf{q}, i\nu_l) \right]_{N, N'} = T \sum_{\mathbf{k}, \omega_{l'}} \gamma_{\text{s}, N}(\mathbf{k}) \gamma_{\text{s}, N'}(\mathbf{k}) G_{\mathbf{k}+\mathbf{q}/2, \text{n}}(i\omega_{l'} + i\nu_l) G_{-\mathbf{k}+\mathbf{q}/2, \text{n}}(-i\omega_{l'}), \quad (17)$$

$$\left[\hat{\Pi}_{\text{t}}^{(0, \pm 1)}(\mathbf{q}, i\nu_l) \right]_{N, N'} = T \sum_{\mathbf{k}, \omega_{l'}} \gamma_{\text{t}, N}(\mathbf{k}) \gamma_{\text{t}, N'}(\mathbf{k}) G_{\mathbf{k}+\mathbf{q}/2, \text{n}}(i\omega_{l'} + i\nu_l) G_{-\mathbf{k}+\mathbf{q}/2, \text{p}}(-i\omega_{l'}), \quad (18)$$

where $N, N' = 1, 2, \dots, N_{\text{max}}$.

Since we are considering the spin-unpolarized case, Eqs. (15)-(18) are spin-independent. We briefly note that the first order correction $\text{Tr}[\hat{\eta}_{\alpha} \hat{\Pi}_{\alpha}^{(m)}(\mathbf{q}, i\nu_l)]$ is already involved in the Hartree self-energy $\Sigma_i^{\text{H}}(\mathbf{p})$ [14], so that we have removed it in Eq.(14) to avoid double counting.

D. Critical Temperature

The critical temperatures of the 1S_0 neutron superfluidity (T_{c}^{nn}), 1S_0 proton superconductivity (T_{c}^{pp}) and 3S_1 deuteron condensation (T_{c}^{d}), as functions of baryon density are obtained from the Thouless criterion [35]. Here, we introduce the Thouless determinant $D_{\alpha}^{(m)}(T)$ defined by

$$D_{\text{s}}^{(-1)}(T) \equiv \det[1 + \hat{\eta}_{\text{s}} \hat{\Pi}_{\text{s}}^{(-1)}(\mathbf{q} = 0, i\nu_l = 0)] = 0 \quad \text{at } T = T_{\text{c}}^{\text{nn}}, \quad (19)$$

$$D_{\text{s}}^{(+1)}(T) \equiv \det[1 + \hat{\eta}_{\text{s}} \hat{\Pi}_{\text{s}}^{(+1)}(\mathbf{q} = 0, i\nu_l = 0)] = 0 \quad \text{at } T = T_{\text{c}}^{\text{pp}}, \quad (20)$$

$$D_{\text{t}}^{(0, \pm 1)}(T) \equiv \det[1 + \hat{\eta}_{\text{t}} \hat{\Pi}_{\text{t}}^{(0, \pm 1)}(\mathbf{q} = 0, i\nu_l = 0)] = 0 \quad \text{at } T = T_{\text{c}}^{\text{d}}. \quad (21)$$

We briefly note that Eqs. (19)-(21) originate from a “block diagonalized” matrix pair-correlation function with respect to $m = \pm 1, 0$, so that the Thouless criterion is decomposed into the three equations (19)-(21). We actually solve them, together with the particle number equation for the nucleon density,

$$\rho_i = -\frac{\partial \Omega}{\partial \mu_i}. \quad (22)$$

In this paper, we approximate $\Sigma_i^H(\mathbf{p})$ to the value at the Fermi surface (for theoretical backfround, see Appendix A). Then, we have

$$\Sigma_i^H(\mathbf{p}) \simeq \Sigma_i^H(\mathbf{p} = \mathbf{k}_{F,i}) \equiv \bar{\Sigma}_i^H, \quad (23)$$

where $k_{F,i}$ is the nucleon Fermi momentum. Introducing the effective chemical potential

$$\mu_i^H \equiv \mu_i - \bar{\Sigma}_i^H, \quad (24)$$

one can write the particle number equation in the form,

$$\rho_i = \rho_i^H + \sum_{i'} \delta \rho_{i'}^{\text{NSR}} L_{i'i}, \quad (25)$$

where the Hartree density ρ_i^H and the NSR correction $\delta \rho_i^{\text{NSR}}$ are, respectively, given by

$$\rho_i^H = 2 \sum_{\mathbf{p}} \rho_{\mathbf{p},i}^H, \quad \delta \rho_i^{\text{NSR}} = -\frac{\partial(\delta \Omega_{\text{NSR}})}{\partial \mu_i^H}. \quad (26)$$

The NSR correction $\delta \rho_i^{\text{NSR}}$ to the number equation involves the diagonal and off-diagonal component of the matrix,

$$L_{ij} = \delta_{ij} - \frac{\partial \bar{\Sigma}_i^H}{\partial \mu_j}. \quad (27)$$

This correction naturally arises from $\delta \Omega_{\text{NSR}}$, whereas it was ignored in the previous work [23, 31, 32, 36]. We note that L_{ij} is related to the compressibility matrix K_{ij}^H in the mean-field approximation as

$$K_{ij}^H \equiv \frac{\partial \rho_i^H}{\partial \mu_j} = -T \sum_{\mathbf{p}, \omega_l} [G_{\mathbf{p},i}(i\omega_n)]^2 L_{ij}, \quad (28)$$

which indicates that L_{ij} corresponds to the vertex correction to the density correlation function. The explicit form of L_{ij} is given by

$$\begin{pmatrix} L_{nn} & L_{np} \\ L_{pn} & L_{pp} \end{pmatrix} = \frac{1}{(1 + \kappa_n)(1 + \kappa_p) - \chi_n \chi_p} \begin{pmatrix} 1 + \kappa_p & -\chi_p \\ -\chi_n & 1 + \kappa_n \end{pmatrix}, \quad (29)$$

where

$$\kappa_i = -T \sum_{\mathbf{p}, \omega_l} V_D^{\text{SEP}}(\bar{k}, \bar{k}) [G_{\mathbf{p}, i}(i\omega_n)]^2, \quad (30)$$

$$\chi_i = -T \sum_{\mathbf{p}, \omega_l} V_{\text{OD}}^{\text{SEP}}(\bar{k}, \bar{k}) [G_{\mathbf{p}, i}(i\omega_n)]^2, \quad (31)$$

with $\bar{k} = |\mathbf{k}_{\text{F}, i} - \mathbf{p}|/2$.

The asymmetric nuclear matter can conveniently be characterized by the total baryon density ρ and the proton fraction Y_p , respectively given by

$$\rho = \rho_n + \rho_p, \quad Y_p = \frac{\rho_p}{\rho_n + \rho_p}. \quad (32)$$

Below, we treat ρ and Y_p as independent parameters, to study their effects on the critical temperatures, T_c^{nn} , T_c^{d} , and T_c^{pp} . We briefly note that, in real neutron star matter, the charge neutrality as well as the chemical equilibrium conditions among protons, neutrons, electrons and muons provide a constraint between ρ and Y_p [42].

III. RESULTS

We start from the superfluid phase transition temperature T_c^{nn} in pure neutron matter ($Y_p = 0$) which has been studied in different levels of theoretical sophistication before. Figure 3 (a) shows theoretical estimates of T_c^{nn} [37]. The NSR result of the rank-three separable potential (“SEP3”) shows good agreement with the previous work of NSR with an effective low-momentum interaction $V_{\text{low}-k}$ based on the renormalization group [36], as well as the result of the lattice Monte-Carlo simulations for the pionless effective field theory [38] shown by the filled circle (where the interaction is chosen so as to reproduce the nn scattering length and the nn effective range).

To see effects of the effective range and the short-range repulsion in the 1S_0 nn channel, we also plot in Fig. 3 (a) the calculated T_c^{nn} of NSR with the contact-type interaction $V_s(k, k') = u_{s,1}^2$ (“contact”), where $u_{s,1}$ is chosen so as to reproduce a_s , and the rank-one separable interaction (“SEP1”). In the low-density regime ($\rho/\rho_0 < 0.01$) including the neutron drip density $\rho_{\text{drip}}/\rho_0 \simeq 1.5 \times 10^{-3}$ [2], all four theoretical calculations agree well with each other and with the Monte Carlo data, indicating that the critical temperature is determined only by the scattering length. The non-zero effective range ($r_s = 2.8$ fm)

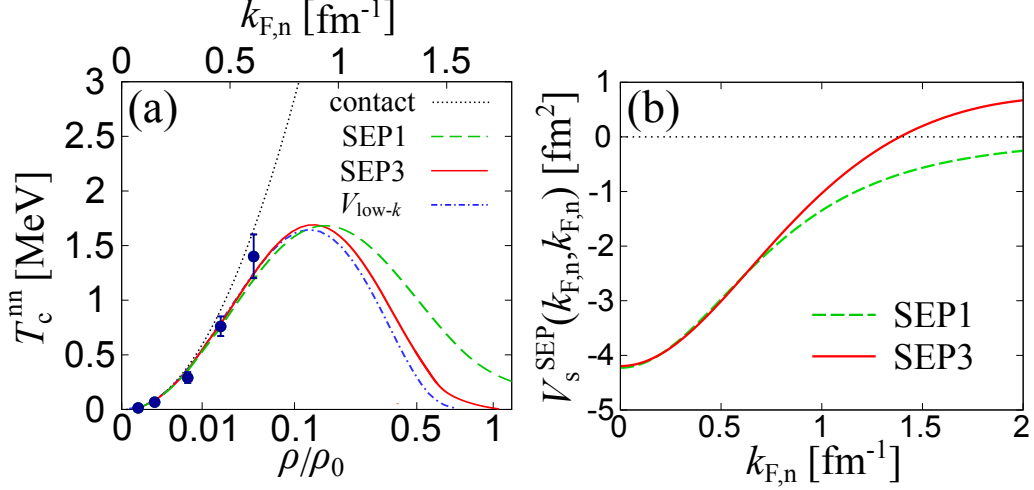


FIG. 3: (a) Calculated 1S_0 neutron superfluid phase transition temperature T_c^{nn} as a function of a nucleon density $\rho = \rho_n$ in pure neutron matter. $k_{\text{F,n}} = (3\pi^2\rho_n)^{\frac{1}{3}}$ is the neutron Fermi momentum. The dotted, dashed, and solid lines denote the NSR results of the contact-type (“contact”), rank-one separable (“SEP1”), and rank-three separable (“SEP3”) interactions, respectively. “ $V_{\text{low-}k}$ ” (dot-dashed line) corresponds to the previous NSR work of the renormalization-group based low-momentum interaction [36]. The filled circles represent the result of the lattice Monte-Carlo simulation for the pionless effective theory [38]. (b) The strength of the nn interaction on the Fermi surface, as a function of the neutron Fermi momentum.

suppresses T_c^{nn} when $\rho/\rho_0 \gtrsim 0.1$ [see Fig. 3 (a)]. It can also be understood as effects of the momentum cut-off $\Lambda_{\text{s},1}$ associated with the effective range [14, 39]. In such a region, the Thouless criterion is approximately given by

$$1 \simeq V_s^{\text{SEP}}(k_{\text{F,n}}, k_{\text{F,n}}) \sum_{\mathbf{k}} \frac{1}{2\xi_{\mathbf{k},\text{n}}} \tanh\left(\frac{\xi_{\mathbf{k},\text{n}}}{2T_c^{\text{nn}}}\right). \quad (33)$$

From Eq. (33), one can find that the nn interaction strength on the Fermi surface $V_s^{\text{SEP}}(k_{\text{F,n}}, k_{\text{F,n}})$ is of importance to evaluate T_c^{nn} . Figure 3 (b) shows $V_s^{\text{SEP}}(k_{\text{F,n}}, k_{\text{F,n}})$ of SEP1 and SEP3. Since $V_s^{\text{SEP}}(k, k')$ of SEP1 and SEP3 are given by Eqs. (6) and (8), respectively, $V_s^{\text{SEP}}(k_{\text{F,n}}, k_{\text{F,n}})$ decreases with increasing $k_{\text{F,n}}$. The decrease of $V_s^{\text{SEP}}(k_{\text{F,n}}, k_{\text{F,n}})$ is associated with $\Lambda_{\text{s},1} \simeq 3/2r_s$. We briefly note that such a decrease does not occur in the case of the contact-type interaction which is momentum-independent. Moreover, the short-range repulsion of the nn interaction takes over for $\rho/\rho_0 > 0.54$ (near the crust-core transition density $\rho/\rho_0 \sim 0.5$ [3]) to further suppress T_c^{nn} as $V_{\text{low-}k}$ and SEP3 shown in Fig.3 (a). In-

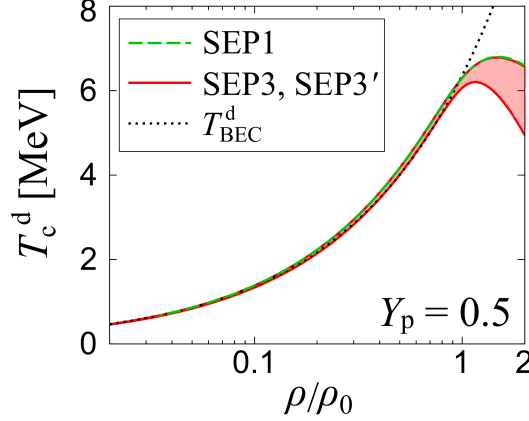


FIG. 4: The deuteron condensation temperature T_c^d in the 3S_1 channel in symmetric nuclear matter ($Y_p = 0.5$). The upper and lower bounds of the solid band correspond to the results using the parameter sets shown in Tables I and II, that is, SEP3 and SEP3', respectively. T_{BEC}^d shows the Bose-Einstein condensation temperature of deuteron gases where the deuteron is assumed as a noninteracting boson.

deed, the comparison of SEP1 and SEP3 interactions on the Fermi surface $V_s^{\text{SEP}}(k_{F,n}, k_{F,n})$ shown in Fig. 3 (b) indicates that the typical strength of the nn interaction decreases with increasing neutron density, and turns into repulsive for $k_{F,n} > 1.39 \text{ fm}^{-1}$. Good agreement of our SEP3 result with the previous $V_{\text{low-}k}$ result over the wide range of baryon density indicates the importance of the detailed interaction structure, as well as associated pairing fluctuations to obtain T_c^{nn} .

We proceed to the case of the symmetric nuclear matter ($Y_p = 0.5$). In this case, examining the Thouless criterion for the nn, pp and np pairing channels, we find that the highest critical temperature is always obtained in the deuteron np channel to $\rho/\rho_0 \leq 2$. Figure 4 shows the critical temperature of the deuteron condensation, T_c^d obtained by SEP3 and SEP3' for np interaction with SEP3 for nn and pp interactions. The upper (lower) bound of the red solid band corresponds to SEP3 (SEP3'). The green dashed line represents the result of SEP1. For comparison, we also plot in Fig. 4 the Bose-Einstein condensation temperature of an assumed noninteracting deuteron gas, given by [31, 32, 40]

$$T_{\text{BEC}}^d = \frac{\pi}{m} \left[\frac{\rho_n}{3\zeta(3/2)} \frac{Y_p}{1 - Y_p} \right]^{\frac{2}{3}}. \quad (34)$$

The obtained T_c^d with all separable interaction potentials approaches T_{BEC}^d in the low-density

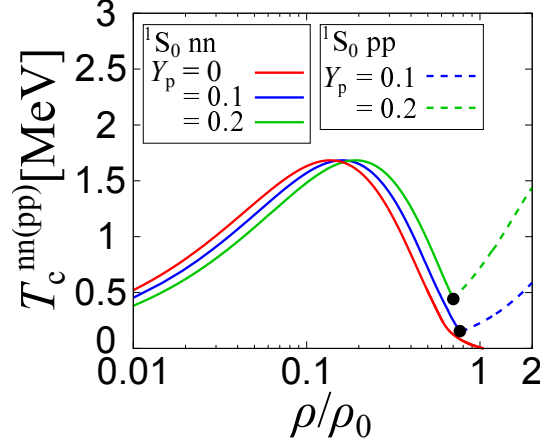


FIG. 5: Calculated critical temperatures T_c^{nn} (solid) and T_c^{pp} (dashed) for 1S_0 neutron superfluid and proton superconductivity. The circles represent the nucleon densities where both superfluid instabilities simultaneously occur.

region. While our result for the symmetric case ($Y_p = 0.5$) is qualitatively consistent with the previous work using different separable interactions within the NSR framework [31, 32], T_c^d has a peak structure at $\rho_{\text{peak}}/\rho_0 > 1$, which is in contrast to the previous work giving $\rho_{\text{peak}}/\rho_0 = 0.3 - 0.8$ [31, 32]. In addition, we do not find a strange back bending behavior of T_c^d seen in [31, 32], irrespective of the use of SEP1, SEP3 and SEP3'. We have not fully understood those differences. However, the treatment of the single-particle energy might be a possible origin.

We now consider asymmetric nuclear matter within the same theoretical framework. We restrict ourselves to the case with the low proton fraction, $Y_p = 0.1 \sim 0.2$, (which is, however, still valid to the study of the neutron star cooling [41–43]). In this range of Y_p , the absolute value of the relative momentum $k = |\mathbf{k}|$ between p and n is smaller than 1.29 fm^{-1} , so that we use SEP3 (which gives better agreement with the empirical phase shift at low energies. The Thouless criterion for the nn, pp and np channels gives the highest critical temperature in the nn channel at low densities, while the pp pairing takes over above the nuclear matter density. Note here that, in the low-density limit, T_{BEC}^d becomes dominant even in asymmetric nuclear matter $0 < Y_p < 0.5$ (see Appendix B). The deuteron pairing is remarkably suppressed due to imbalanced Fermi surfaces. Figure 5 shows T_c^{nn} and T_c^{pp} in the case of SEP3 [37].

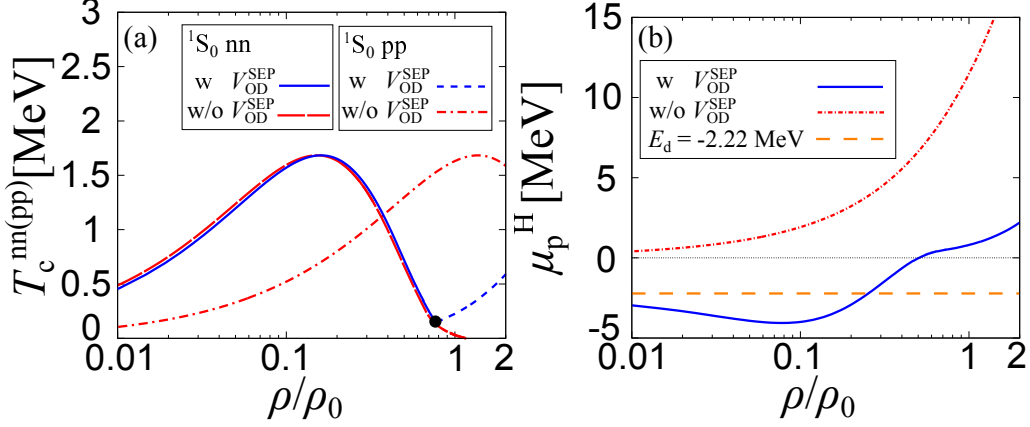


FIG. 6: (a) The critical temperatures $T_c^{nn(pp)}$, and (b) the effective proton chemical potential $\mu_p^H = \mu_p - \bar{\Sigma}_p^H$, at $Y_p = 0.1$ with and without the off-diagonal np interaction V_{OD}^{SEP} . The horizontal dashed line in panel (b) represents the deuteron binding energy $E_d = -2.22$ MeV.

In Fig. 5, with increasing the proton fraction Y_p , the peak of T_c^{nn} is found to gradually move to higher density. This is simply because the neutron density decreases as $\rho_n = (1 - Y_p)\rho$, so that the whole curve of T_c^{nn} shifts to the right. The black circle in Fig. 5 indicates the density at which T_c^{pp} exceeds T_c^{nn} when $Y_p > 0$. Beyond this, the pp interaction becomes more attractive, due to relatively small proton Fermi momentum $k_{F,p} = (3\pi^2\rho_p)^{\frac{1}{3}} = (3\pi^2\rho Y_p)^{\frac{1}{3}}$, while the nn interaction is strongly suppressed by the short-range repulsion due to large neutron Fermi momentum $k_{F,n} = (3\pi^2\rho_n)^{\frac{1}{3}} = [3\pi^2\rho(1 - Y_p)]^{\frac{1}{3}}$. At higher density, T_c^{pp} would also be suppressed, but it is beyond the applicability of the present formalism (see Appendix B).

To see effects of strong np interactions, we plot the critical temperatures T_c^{nn} , as well as, T_c^{pp} in Fig. 6 (a). We also show the effective proton chemical potential μ_p^H which is defined in Eq.(24) (at $T = T_c^{nn}$, below $0.77\rho_0$ and at $T = T_c^{pp}$ above $0.77\rho_0$), with and without the np interaction, V_{OD}^{SEP} in Figs. 6 (b). We find that while T_c^{nn} is insensitive to the strength of the np interaction, T_c^{pp} is substantially affected. The latter can be understood by the behavior of μ_p^H . When $V_{OD}^{SEP} = 0$, μ_p^H is always positive as shown in Figs. 6 (b), indicating that the proton Fermi surface is formed, irrespective of the value of baryon density ρ , naturally leading to the proton superconductivity. On the other hand, when $V_{OD}^{SEP} \neq 0$, the strong np interaction in the deuteron channel reduces μ_p^H in the low-density region, to eventually approach the deuteron binding energy $E_d = -2.22$ MeV in the low-density limit. As a

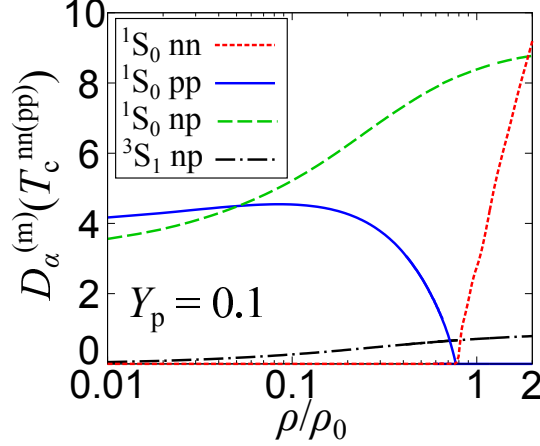


FIG. 7: Thouless determinants, $D_\alpha^{(m)}$ in all four channels as functions of the baryon density ρ with $Y_p = 0.1$ at $T = T_c^{\text{nn}}$ below $\rho = 0.77\rho_0$ and at $T = T_c^{\text{pp}}$ above $\rho = 0.77\rho_0$. The dotted, solid, dashed, and dot-dashed lines represent $D_\alpha^{(m)}$ of the 1S_0 nn, 1S_0 pp, 1S_0 np, and 3S_1 np channels, respectively.

result, the pp pairing does not take place. In the low density limit with $0 < Y_p < 0.5$, one finds $\mu_n \sim \mu_n^H \rightarrow 0$ and $\mu_p \sim \mu_p^H \rightarrow E_d$ [40] as in the case of an asymmetric two-component Fermi atomic gas [44].

Figure 7 shows the Thouless determinants $D_\alpha^{(m)}(T)$ in Eqs. (19)-(21) for $Y_p = 0.1$ at $T = T_c^{\text{nn}}$ below $0.77\rho_0$, and at $T = T_c^{\text{pp}}$ above $0.77\rho_0$. When $D_\alpha^{(m)}(T)$ becomes smaller to vanish, pairing fluctuations become stronger and eventually diverge at the second-order superfluid/superconducting phase transition. Such diverging fluctuations can be seen in the 1S_0 nn channel for $\rho < 0.77\rho_0$, as well as in the 1S_0 pp channel for $\rho > 0.77\rho_0$. On the other hand, pairing fluctuations in the 1S_0 np channel are weak, compared to the other channels. The Thouless determinant in the 3S_1 np channel is close to zero over the entire density, but the deuteron condensation does not occur when $Y_p = 0.1$, because of the large difference of the chemical potentials between neutrons and protons. Nevertheless, strong pairing fluctuations in the deuteron channel play a crucial role for T_c^{pp} , as seen in Fig.6.

Before ending this section, we discuss the possibility of a Fulde-Ferrell-Larkin-Ovchinnikov (FFLO) state [45–48] in the deuteron channel for $0 < Y_p < 0.2$ (which is relevant for neutron stars). The FFLO state may occur, when two kinds of fermions attractively interact with each other in the presence of population imbalance. In such a case, the Cooper pairs

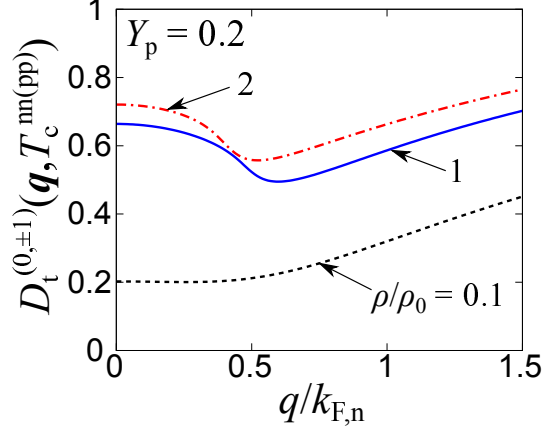


FIG. 8: Thouless determinant in the deuteron channel as a function of the center-of-mass momentum q at $Y_p = 0.2$ for different values of the baryon density.

with a non-zero center-of-mass momentum are formed. In the present case, the Thouless determinant at a non-zero momentum [49, 50], $D_t^{(0,±1)}(\mathbf{q}, T) = \det[1 + \hat{\eta}_t \hat{\Pi}_t^{(0,±1)}(\mathbf{q}, i\nu_l = 0)]$ is an appropriate measure. Figure 8 shows the center-of-mass momentum ($q = |\mathbf{q}|$) dependence of $D_t^{(0,±1)}(\mathbf{q}, T)$ at $T = T_c^{nn(pp)}$ in asymmetric nuclear matter with $Y_p = 0.2$. We find that $D_t^{(0,±1)}(\mathbf{q}, T)$ takes a minimum at a non-zero momentum q^* in the high-density region ($\rho > \rho_0$). Indeed, q^* at $\rho = \rho_0$ in Fig.8 is close to the typical momentum of the FFLO pairing, $k_{F,n}^{\text{eff}} - k_{F,p}^{\text{eff}} = (2m\mu_n^H)^{\frac{1}{2}} - (2m\mu_p^H)^{\frac{1}{2}} \simeq 0.7k_{F,n}$. Although $D_t^{(0,±1)}(q^*, T)$ is still far away from zero, it may be interpreted as a precursor of the FFLO state at larger Y_p .

IV. CONCLUDING REMARKS

In this paper, we have extended the Nozières-Schmitt-Rink approach to four-component fermion system, to examine the superfluid phase transition at finite temperatures in asymmetric nuclear matter at nuclear and subnuclear densities. Including pairing fluctuations in the S -wave neutron-neutron, proton-proton, and neutron-proton channels, we evaluated the critical temperature of 1S_0 neutron superfluidity T_c^{nn} and proton superconductivity T_c^{pp} . We clarified effects of strong neutron-proton pairing fluctuations in the deuteron channel. While resultant T_c^{nn} in pure neutron matter agrees well with the previous Monte Carlo data in the low baryon-density region, it is remarkably suppressed around the nuclear saturation density ρ_0 , due to the short-range nn repulsion. We found that T_c^{pp} at low-density is substantially

suppressed by the neutron-proton pairing fluctuations.

There are several future directions to be explored on the basis of the framework developed in this paper.

1. We have focused on the superfluid/superconducting instability in the normal phase throughout the paper. However, the present model together with the framework of Ref. [14] can be combined to study the superfluid phase below the critical temperature, such as equation of state, as well as magnitude of the pairing gap.
2. To improve the accuracy of $T_c^{\text{nn,pp,d}}$, we need to include the coupled 3S_1 - 3D_1 channel potential beyond the present 3S_1 channel potential. Such a channel-coupling introduces extra in-medium effect associated with the Pauli blocking by the intermediate 3D_1 state.
3. There are correlations which are ignored in the present paper, such as Gorkov and Melik-Barkhudarov (GMB) screening [51–53], as well as the competition between the screening and anti-screening corrections [54, 55].
4. The nn pairing in the 3P_2 channel [3, 56–58] would cause a dominant superfluid component in the liquid core of neutron stars. Introducing a separable interaction in the P -wave channel and applying the present framework would be a first step toward the analysis of such unconventional superfluids.

Acknowledgments

We thank G. Baym, S. Furusawa, S. Han, K. Iida, D. Inotani, T. Kunihiro, H. Liang, P. Naidon, A. Ohnishi, P. Pieri, G. C. Strinati, H. Togashi, and N. Yamamoto for useful discussions. H. T. was supported by a Grant-in-Aid for JSPS fellows (No.17J03975). T. H. was supported by RIKEN iTHEMS Program. Y. O. was supported by KiPAS project in Keio University. This work was supported by Grant-in-aid for Scientific Research from MEXT and JSPS in Japan (No.JP16K17773, No.JP24105006, No.JP23684033, No.JP15H00840, No.JP15K00178, No.JP16K05503, No.JP18H03712, No.JP18H05236, No.JP18H05406, No.JP18K11345, No.JP19K03689).

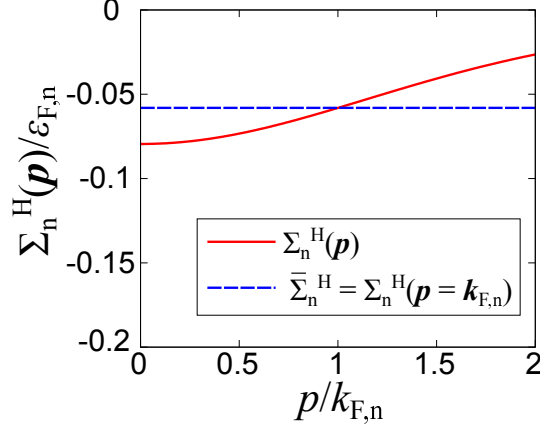


FIG. 9: Hartree self-energy $\Sigma_n^H(\mathbf{p})$ and the approximated Hartree shift $\bar{\Sigma}_n^H = \Sigma_n^H(\mathbf{p} = \mathbf{k}_{F,n})$ in pure neutron matter with SEP at $\rho = 0.29\rho_0$, $\varepsilon_{F,n} = \mu_n$ and $T = 0.1\varepsilon_{F,n}$

Appendix A: The Hartree shift

Figure 9 shows the momentum dependence of the Hartree self-energy $\Sigma_i^H(\mathbf{p})$ in the pure neutron matter at $\rho = 0.29\rho_0$ with SEP1. We set $\varepsilon_{F,n} = \mu_n$ and $T = 0.1\varepsilon_{F,n}$, and pairing-fluctuation effects are neglected for simplicity. The magnitude of the Hartree shift is relatively small compared to the neutron chemical potential μ_n and its momentum dependence is not substantial. Since the momentum at the Fermi surface is the most important for Cooper pairings, we introduce an approximation $\bar{\Sigma}_i^H = \Sigma_i^H(\mathbf{p} = \mathbf{k}_{F,i})$ as adopted in the text.

In general, the momentum dependence of the Hartree self-energy near the Fermi surface gives rise to the effective mass M^* defined by [32]

$$\frac{1}{M^*} = \frac{1}{M} + 2 \left. \frac{\partial \Sigma_i^H(\mathbf{p})}{\partial p^2} \right|_{\mathbf{p}=\mathbf{k}_{F,i}}. \quad (\text{A1})$$

From Fig. 9, we find $M^* \simeq 0.98M$. In the present work, we have not taken into account this small correction.

We note that the present approximation of the Hartree shift is different from the previous work [14], where $\bar{\Sigma}_n^H = V_s(\mathbf{0}, \mathbf{0})\rho_n^H/2 = V_s^{\text{SEP}}(0, 0)\rho_n^H/2$ is used. While such an approximation of the Hartree shift is sufficient enough in the low-density region, it leads to the divergence of L_{ij} near the nuclear saturation density. Furthermore, the present form of the Hartree shift is rather consistent with the mean-field approximation under the separable interaction $V_s^{\text{SEP}}(k, k')$.

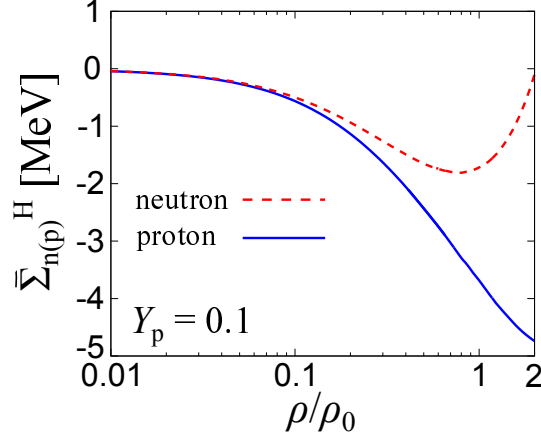


FIG. 10: Thouless determinant in the deuteron channel as a function of the center-of-mass momentum q at $Y_p = 0.2$ for different values of the baryon density.

Figure 10 shows the baryon density dependence of $\bar{\Sigma}_i^H$ in asymmetric nuclear matter with $Y_p = 0.1$. In the low-density limit, the shifts are negligibly small where the interaction can be well approximated by the contact-type interaction. While $\bar{\Sigma}_n^H$ increases around the nuclear matter density due to the short-range repulsion in the 1S_0 nn channel, $\bar{\Sigma}_p^H$ decreases further, reflecting the difference between $k_{F,p}$ and $k_{F,n}$. In addition, the behavior of $\bar{\Sigma}_p^H$ is mainly dictated by the 3S_1 np interaction rather than the 1S_0 pp interaction because of $\rho_n > \rho_p$ in neutron star matter.

Appendix B: T_c^{pp} and T_c^d at higher and lower densities

Since our separable interactions are adjusted so as to reproduce the AV18 phase shift up to $k = 2 \text{ fm}^{-1}$, they cannot be used to investigate the properties of neutron matter above $\rho = 1.59\rho_0$ (where $k_{F,n} = 2 \text{ fm}^{-1}$). On the other hand, the effective pp interaction $V_s^{\text{SEP}}(k_{F,p}, k_{F,p})$ at the proton Fermi momentum $k_{F,p}$ is still in the range of $0 \leq k_{F,p} \leq 2 \text{ fm}^{-1}$ even up to $\rho = 15.9\rho_0$ in the case of $Y_p = 0.1$. Therefore, just to see the qualitative behavior at high density, we plot T_c^{pp} up to $5\rho_0$ in Fig. 11. The result exhibits an upturn behavior in higher density regime due to the effective-range correction as well as short-range repulsion in the 1S_0 pp channel. The 3S_1 np interaction modifies its density dependence through the suppression of the effective proton chemical potential μ_p^H as shown in Fig. 6 (b).

On the other hand, in the low-density limit, T_{BEC}^d exceeds T_c^{nn} in the case of a finite

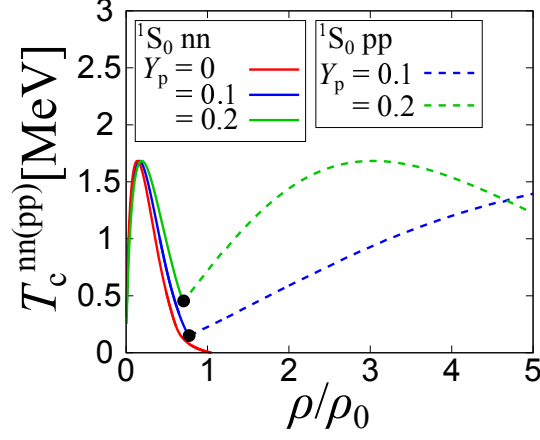


FIG. 11: Calculated critical temperature $T_c^{\text{nn(pp)}}$ of the 1S_0 neutron superfluidity (proton superconductivity) in asymmetric nuclear matter up to $\rho = 5\rho_0$.

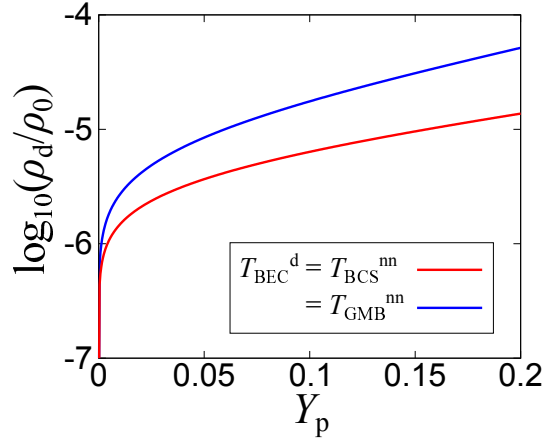


FIG. 12: The proton fraction dependence of the critical nucleon density ρ_d where $T_{\text{BEC}}^d = T_{\text{BCS}}^{\text{nn}}$ and $T_{\text{BEC}}^d = T_{\text{GMB}}^{\text{nn}}$.

proton fraction. In this limit, T_c^{nn} is given by the zero-range BCS result

$$T_{\text{BCS}}^{\text{nn}} = \frac{8e^\gamma}{\pi e^2} \varepsilon_{\text{F,n}} e^{\frac{\pi}{2k_{\text{F,n}} a_s}}. \quad (\text{B1})$$

where $\gamma = 0.577$ is the Euler constant. Since T_c^d is equal to T_{BEC}^d given by Eq. (34) due to the large binding energy $|E_d| = 2.22$ MeV, we can analytically obtain the critical nucleon density ρ_d where $T_{\text{BEC}}^d = T_{\text{BCS}}^{\text{nn}}$ as

$$\rho_d = \frac{\pi}{24a_s^3(1 - Y_p)} \left[2 \ln \left(\frac{\pi}{2} \right) + 2 - \gamma + \frac{2}{3} \ln \left(\frac{1}{9\pi^2 \zeta(3/2)} \frac{Y_p}{1 - Y_p} \right) \right]^{-3}. \quad (\text{B2})$$

Figure 12 shows the proton fraction dependence of ρ_d . We also plot ρ_d obtained from the GMB result $T_{\text{BEC}}^d = T_{\text{GMB}}^{\text{nn}} = (4e)^{-1/3} T_{\text{BCS}}^{\text{nn}}$ in the presence of the screening correction [51]. In the relevant region for a neutron star ($0 < Y_p < 0.2$), ρ_d is smaller than the neutron drip density $\rho_{\text{drip}}/\rho_0 = 1.5 \times 10^{-3}$ [2]. We note that Eq. (B2) is valid at small proton fraction ($Y_p < 0.2$), where ρ_d appears in the sufficiently low-density regime $[(k_{\text{F,n}} a_s)^{-1} < -1]$ [40].

-
- [1] T. Takatsuka and R. Tamagaki, Prog. Theor. Phys. Suppl. **112**, 27 (1993).
 - [2] D.-J. Dean and M. Hjorth-Jensen, Rev. Mod. Phys. **75**, 607 (2003).
 - [3] D. Page, J. M. Lattimer, M. Prakash, and A. W. Steiner, in *Novel Superfluids*, edited by K. H. Bennemann and J. B. Ketterson (Oxford University Press, Oxford, 2014).
 - [4] M. Oertel, M. Hempel, T. Klähn, S. Typel, Rev. Mod. Phys. **89**, 015007 (2017).
 - [5] G. Baym, T. Hatsuda, T. Kojo, P. D. Powell, Y. Song and T. Takatsuka, Rept. Prog. Phys. **81**, 056902 (2018).
 - [6] J. Carlson, S. Gandolfi and A. Gezerlis, PTEP **2012**, 01A209 (2012).
 - [7] S. Gandolfi, A. Gezerlis, and J. Carlson, Annu. Rev. Nucl. Part. Sci. **65**, 303 (2015).
 - [8] M. Horikoshi, M. Koashi, H. Tajima, Y. Ohashi, and M. Kuwata-Gonokami, Phys. Rev. X **7**, 041004 (2017).
 - [9] M. Horikoshi and M. Kuwata-Gonokami, Int. J Mod. Phys. E **28**, 1930001 (2019).
 - [10] G. C. Strinati, P. Pieri, G. Röpke, P. Schuck, and M. Urban, Phys. Rep. **738**, 1 (2018).
 - [11] C. Chin, R. Grimm, P. Julienne, and E. Tiesinga, Rev. Mod. Phys. **82**, 1225 (2010).
 - [12] E. J. Mueller, Rep. Prog. Phys. **80**, 104401 (2017).
 - [13] S. Jensen, C. N. Gilbreth, and Y. Alhassid, Eur. Phys. J. Spec. Top. **227**, 2241 (2019).
 - [14] P. van Wyk, H. Tajima, D. Inotani, A. Ohnishi, and Y. Ohashi, Phys. Rev. A **97**, 013601 (2018).
 - [15] P. Nozières and S. Schmitt-Rink, J. Low Temp. Phys. **59**, 195 (1985).
 - [16] Y. Yamaguchi, Phys. Rev. **95**, 1628 (1954).
 - [17] T. R. Mongan, Phys. Rev. **175**, 1260 (1968).
 - [18] T. R. Mongan, Phys. Rev. **178**, 1597 (1969).
 - [19] L. Mathelitsch, W. Plessas, and W. Schweiger, Phys. Rev. C **26**, 65 (1982).
 - [20] J. Haidenbauer and W. Plessas, Phys. Rev. C **30**, 1822 (1984).

- [21] J. Haidenbauer and W. Plessas, Phys. Rev. C **32**, 1424 (1985).
- [22] P. Grygorov, E. N. E. van Dalen, H. Mütter, and J. Margueron, Phys. Rev. C **82**, 014315 (2010).
- [23] T. Alm, B. L. Friman, G. Röpke, and H. Schulz, Nucl. Phys. A **A551**, 45 (1993).
- [24] A. Osman, Phys. Rev. C **19**, 1127 (1979).
- [25] A. Schnell, G. Röpke, and P. Schuck, Phys. Rev. Lett. **83**, 1926 (1993).
- [26] A. D. Sedrakian, D. Blaschke, G. Röpke, and H. Schulz, Phys. Lett. B **338**, 111 (1994).
- [27] M. Beyer, G. Röpke, and A. Sedrakian, Phys. Lett. B **376**, 7 (1996).
- [28] W. Schadow, W. Sandhas, J. Haidenbauer, and A. Nogga, Few-Body Syst. **28**, 241 (2000).
- [29] P. Bożek and P. Czerski, Eur. Phys. J. A **qq**, 271 (2001).
- [30] Y. Dewulf, W. H. Dickhoff, D. Van Neck, E. R. Stoddard, and M. Waroquier, Phys. Rev. Lett. **90**, 152501 (2003).
- [31] H. Stein, A. Schnell, T. Alm and G. Röpke, Z. Phys. A **351**, 295 (1995)
- [32] M. Jin, M. Urban, and P. Schuck, Phys. Rev. C **82**, 024911 (2010).
- [33] N. Martin and M. Urban, Phys. Rev. C **90**, 065805 (2014).
- [34] R. B. Wiringa, V. G. J. Stoks, and R. Schiavilla, Phys. Rev. C **51**, 38 (1995).
- [35] D. J. Thouless, Annals of Physics **10**, 553 (1960).
- [36] S. Ramanan and M. Urban, Phys. Rev. C **88**, 054315 (2013).
- [37] We note that since the calculation of T_c within SEP3 in the high density region $k_{F,n} \gtrsim 1.3$ fm⁻¹ of pure neutron matter is numerically demanding, we extrapolate them to $k_{F,n} = 1.73$ fm⁻¹ where T_c invariably disappears because the phase shift at $k = k_{F,n}$ becomes zero there, by using the Padé approximation.
- [38] T. Abe and R. Seki, Phys. Rev. C **79**, 054003 (2009).
- [39] N. Andrenacci, A. Perali, P. Pieri, and G. C. Strinati, Phys. Rev. B **60**, 12 410 (1999).
- [40] H. Tajima, T. Hatsuda and Y. Ohashi, J. Phys.: Conf. Ser. **969**, 012003 (2018).
- [41] J. M. Lattimer, C. J. Pethick, M. Prakash, and P. Haensel, Phys. Rev. Lett. **66**, 2701 (1991).
- [42] A. Akmal, V. Pandharipande, and D. Ravenhall, Phys. Rev. C **58**, 1804 (1998).
- [43] M. G. Alford and S. P. Harris, Phys. Rev. C **98**, 065806 (2018).
- [44] X.-J. Liu and H. Hu, Europhys. Lett. **75**, 364 (2006).
- [45] P. Fulde and R. A. Ferrell, Phys. Rev. **135**, A550 (1964).
- [46] A. I. Larkin and Y. N. Ovchinnikov, Sov. Phys. JETP **20**, 762 (1965).

- [47] L. Radzihovsky and D. E. Sheehy, Rep. Prog. Phys. **73**, 076501 (2010).
- [48] L. Radzihovsky, Phys. Rev. A **84**, 023611 (2011).
- [49] Y. Ohashi, J. Phys. Soc. Jpn. **71**, 2625 (2002).
- [50] B. Frank, J. Lang, and W. Zwerger, J. Exp. Theor. Phys. **127**, 812 (2018).
Phys. Rev. C **64**, 064314 (2001).
- [51] L. P. Gorkov and T. K. Melik-Barkhudarov, Sov. Phys. JETP **13**, 1018 (1961) [Zh. Eksp. Teor. Fiz. **40**, 1452 (1961)].
- [52] Z.-Q. Yu, K. Huang, and L. Yin, Phys. Rev. A **79**, 053636 (2009).
- [53] L. Pisani, A. Perali, P. Pieri, and G. C. Strinati, Phys. Rev. B **97**, 014528 (2018).
- [54] L. G. Cao, U. Lombardo, and P. Schuck, Phys. Rev. C **74**, 064301 (2006).
- [55] S. Ramanan and M. Urban, Phys. Rev. C **98**, 024314 (2018).
- [56] R. Tamagaki, Prog. Theor. Phys. **44**, 905 (1970).
- [57] M. Hoffberg, A. E. Glassgold, R. W. Richardson, and M. Ruderman, Phys. Rev. Lett. **24**, 775 (1970).
- [58] T. Takatsuka, Prog. Theor. Phys. . **48**, 1517 (1972).